Deep ocean heat content changes estimated from observation and reanalysis product and their influence on sea level change

Shinya Kouketsu,[1] Toshimasa Doi,[1] Takeshi Kawano,[1] Shuhei Masuda,[1] Nozomi Sugiura,[2] Yuji Sasaki,[2] Takahiro Toyoda,[3] Hiromichi Igarashi,[2] Yoshimi Kawai,[1] Katsuro Katsumata,[1] Hiroshi Uchida,[1] Masao Fukasawa,[1] and Toshiyuki Awaji[2,4]

Received 11 June 2010; revised 24 November 2010; accepted 28 December 2010; published 5 March 2011.

[1] We calculated basin-scale and global ocean decadal temperature change rates from the 1990s to the 2000s for waters below 3000 m. Large temperature increases were detected around Antarctica, and a relatively large temperature increase was detected along the northward path of Circumpolar Deep Water in the Pacific. The global heat content (HC) change estimated from the temperature change rates below 3000 m was 0.8×10^{22} J decade^{-1}; a value that cannot be neglected for precise estimation of the global heat balance. We reproduced the observed temperature changes in the deep ocean using a data assimilation system and examined virtual observations in the reproduced data field to evaluate the uncertainty of the HC changes estimated from the actual temporally and spatially sparse observations. From the analysis of the virtual observations, it is shown that the global HC increase below 3000 m during recent decades can be detected using the available observation system of periodic revisits to the same sampling sections, although the uncertainty is large.

Citation: Kouketsu, S., et al. (2011), Deep ocean heat content changes estimated from observation and reanalysis product and their influence on sea level change, *J. Geophys. Res.*, *116*, C03012, doi:10.1029/2010JC006464.

1. Introduction

[2] Global heat budgets are important for understanding global climate variability. The estimation of ocean heat content (HC) change is critically important for assessing the imbalance of the earth's heat budget, which coincides with air temperature increases in recent decades [*Hansen et al.*, 2005; *Douglass and Knox*, 2009]. *Willis et al.* [2004] reported that the oceanic heat uptake in the upper 750 m from 1993 to 2003 corresponded to a heat flux of 0.86 W m^{-2} through the ocean surface. *Levitus et al.* [2005] showed that a large amount of heat (14.5×10^{22} J) was absorbed by the upper 3000 m of the ocean from 1955 to 1998. The HC change contributes to sea level rise [e.g., *Domingues et al.* 2008]; the contribution from the HC changes in the upper 3000 m was about half of the total sea level rise from 1993 to 2003, which is estimated from satellite measurements to be 3.1 mm yr^{-1} [*Bindoff et al.*, 2007]. However, the HC changes deeper than 3000 m and their contribution to sea level rise are not well known. For an accurate estimation of the oceanic heat budget, it is important to include the heat budget in the deep ocean, even though almost all of the changes in ocean HC are confined to the upper 750 m [*Hansen et al.*, 2005].

[3] Because the temperature variability is small in the deep ocean, data of the highest accuracy are necessary to evaluate the HC change there. Thus, almost all studies of temperature changes in the deep ocean have used the carefully processed data collected under the World Ocean Circulation Experiment (WOCE) Hydrographic Programme (WHP) and revisit cruises. Warming near the bottom was reported in many basins from comparisons of WHP and revisit data [e.g., *Fukasawa et al.*, 2004; *Johnson and Doney*, 2006; *Kawano et al.*, 2006; *Johnson et al.*, 2007, 2008]. Although the careful analyses in these previous studies detected significant temperature differences near the bottom, the HC changes in the global deep ocean were not well described.

[4] *Purkey and Johnson* [2010] recently reported for the first time the basin-scale HC changes in the deep ocean to investigate a role of recent warming of Antarctic waters in global heat and sea level budgets. They divided the world ocean into 32 deep basins separated by topography, and estimated a temperature trend and confidence intervals for each basin using hydrographic observations from within each basin. They found that substantial warming around Antarctica was important for estimates of global energy budgets. However, they did not describe the spatial pattern of HC change at subbasin scales, especially in the Pacific, as they divided the global deep ocean into large basins.

[1]Research Institute for Global Change, JAMSTEC, Yokosuka, Japan.
[2]Data Management and Engineering Department, Data Research Center for Marine-Earth Sciences, JAMSTEC, Yokohama, Japan.
[3]Meteorological Research Institute, Ibaraki, Japan.
[4]Department of Geophysics, Kyoto University, Kyoto, Japan.

0148-0227/11/2010JC006464

Table 1. WOCE Sections Used as Data Sources for This Study[a]

Ocean Basin	Line Name	Initial Survey	Revisit
Pacific	P01	1985	1999
	P02	1994	2004
	P03	1985	2005
	P06	1992	2003
	P10	1993	2005
	P14	1992, 1993	2007
	P16	1991	2005, 2006
	P17	1991, 1993	2001
	P18	1994	2008
Atlantic	AR07 (A01)	1990	1996, 1998
	AR19 (A02)	1993	2000
	A05	1992	1998
	A06	1993	2000
	A10	1992	2003
	A12	1992	2000
	A16	1988, 1989	2003, 2005
	A20	1997	2003
	A22	1997	2003
Indian	I03, I04	1995	2003
	I05	1987	2002
	I06	1993	1996
	I09 (I08S)	1994, 1995	2007
Southern	SR01	1993, 1994, 1996, 1997	1993, 1994, 1996, 1997
	SR03	1991, 1993, 1994, 1995, 1996, 2001	1991, 1993, 1994, 1995, 1996, 2001
	SR04	1989, 1990, 1996, 1998	1989, 1990, 1996, 1998

[a]Including section name, year of initial occupation, and year(s) of subsequent occupation(s). The section locations are shown in Figure 1.

[5] The spatial distribution of temperature changes can be a clue to understanding deep ocean circulation and its variability. For almost all of the bottom layer (below 4000 m) of the Pacific Ocean, *Kawano et al.* [2010] showed that the water was warming and suggested that the warming was caused by the reduction in dense water formation near Antarctica, as *Nakano and Suginohara* [2002a] had shown using a numerical model that the reduction in dense water formation near the Adelie Coast resulted in bottom water warming in the Pacific Ocean. *Masuda et al.* [2010] revealed the recent bottom water warming in the Pacific Ocean using an assimilation model and analyzed the mechanisms of the rapid transfer of the warming anomaly from Antarctica to the deep layers of the North Pacific. However, they did not describe the spatial distribution of the HC changes in the Indian and Atlantic oceans, although bottom water warming has also been detected in some parts of these oceans [e.g., *Johnson and Doney*, 2006; *Johnson et al.*, 2008].

[6] There are few estimates of global HC changes in the deep ocean using direct measurements, and the spatial distribution of the changes has not been described in detail. Therefore, for this study, we divided each ocean basin into many "boxes," mapped the temperature changes in those boxes between the 1990s and the 2000s to show their spatial distribution, calculated steric height changes due to salinity changes as well as the temperature changes, and estimated the global and basin-scale HC changes in the deep ocean.

[7] Furthermore, the uncertainty of previous estimates of HC changes in the deep ocean, especially that due to temporal variability, is not clear. *Purkey and Johnson* [2010] estimated 95% confidence intervals for their estimated HC changes, using all hydrographic observations included in the basins, explicitly taking into account a spatial decorrelation length. Because they estimated the confidence intervals using all of the observations carried out in the large basins on different dates, their confidence intervals can include some uncertainties due to temporal variability. However, because most WHP sections were surveyed only twice, it is difficult to evaluate the uncertainty due to temporal variability using only the observational data.

[8] In this study, we evaluate the uncertainty of HC changes in the deep ocean as estimated from WHP and revisit observations by using ocean reanalysis product developed from a global four-dimensional variational (4D-VAR) data assimilation system that can optimally synthesize observations and model results.

2. Methods

2.1. Observations

[9] We used temperature and salinity data collected as part of the WHP conducted from 1985 to 1995 and the revisits after 1997, which are available from the Climate Variability and Predictability (CLIVAR) and Carbon Hydrographic Data Office (CCHDO). The data sets used are listed in Table 1. The uncertainties of temperature and salinity measurements are about 0.001°C and 0.002, respectively [e.g., *Kawano et al.*, 2010]. The uncertainty in temperature measurements was less than the difference detected in the deep ocean (typically below 3000 m) in the comparison between WHP cruises and revisits along many sections, whereas the salinity changes in the deep ocean were too small to detect along many sections [e.g., *Kawano et al.*, 2006; *Kouketsu et al.*, 2009]. Therefore, for this study, we describe the temperature and HC changes in detail and note the effect of salinity changes on the steric height change as well as that of the temperature changes in the deep ocean, focusing on the areas where large salinity changes were detected.

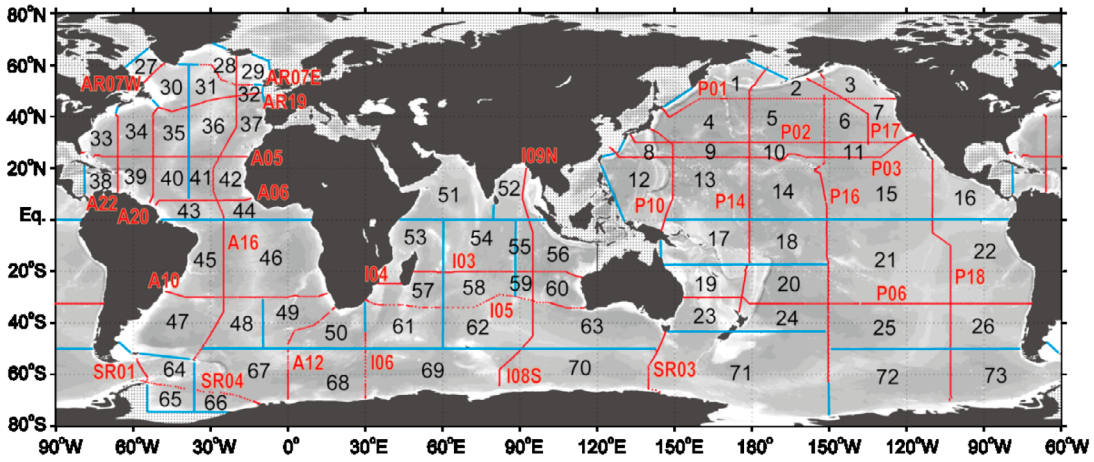

Figure 1. The WOCE Hydrographic Programme (WHP) lines with section names (red) and additional lines (blue) used to divide the world ocean into 73 boxes. The additional lines were chosen to optimize the size of boxes and to exclude marginal seas.

[10] The changes in HC and steric height for the global ocean were calculated for 73 boxes delimited by the intersections of WHP observation lines and some additional lines (Figure 1) that were chosen to allow a detailed description of the horizontal pattern of HC changes. Lines were also added to exclude the shallow seas such as the Bering, East China Sea, and South China Seas. The 5 min gridded world elevation data (ETOPO-5) [*NOAA*, 1988] were used to determine the horizontal and bottom boundaries of each box.

[11] The WHP and revisit cruises were designed to take observations at the same locations. However, slight differences exist in station locations and in the maximum depth of the observations. The data from surveys with a smaller number of stations were interpolated to match the locations of other data, and the maximum depth of observations for each station was set to the shallower depth of the original or revisit survey.

[12] We calculated the temperature changes averaged on the lateral boundaries of 100 m thick layers, and normalized them to a 10 year interval. We then calculated the temperature change rates for the 100 m thick layers in each box by averaging the lateral boundary temperature change rates weighted by the horizontal lengths of the lateral boundaries. The method is described in detail by *Kawano et al.* [2010].

[13] In addition, we calculated 90% confidence intervals using degrees of freedom estimated assuming a spatial decorrelation length of changes in the deep ocean was 160 km, which was used by *Purkey and Johnson* [2010]. Because multiple repeated observations were available for lines SR01, SR03, and SR04, the temperature changes along these lines were calculated for each 100 m thick layer from the linear trends of the repeated observations, and then these values were used in the calculations of temperature changes within the boxes with these lines as boundaries.

2.2. Data Assimilation

[14] The available observational data in the deep ocean are too sparse to determine the temporal variability. Although short-term variability can be assumed to be small in the deep ocean, the magnitude of the variability is unclear and the aliasing effect in the analysis used to describe the long-term changes may not be negligible. Furthermore, estimation with spatially sparse observations can cause a bias in the calculation of HC changes. To evaluate the uncertainty in the observational analysis, we used ocean reanalysis product, which, under realistic surface forcings, reflect most of the familiar gross features of observed bottom water changes reported in previous studies, such as slight temperature warming in the North Pacific and temperature warming on the western side of the South Atlantic [e.g., *Fukasawa et al.*, 2004; *Johnson and Doney*, 2006; *Kawano et al.*, 2010; *Purkey and Johnson*, 2010].

[15] Ocean reanalysis product were derived from a 4D-VAR adjoint data assimilation system, which provides the best time-trajectory fit to observations and can create a dynamically self-consistent data set. The assimilation system was developed under a collaborative program between the Japan Agency for Marine-Earth Science and Technology (JAMSTEC) and Kyoto University [e.g., *Masuda et al.*, 2003] and is based on a global oceanic general circulation model (OGCM): specifically, version 3 of the Geophysical Fluid Dynamics Laboratory (GFDL; NOAA, USA) Modular Ocean Model (MOM) [*Pacanowski and Griffies*, 2000]. The horizontal resolution is 1 degree of latitude and longitude and there are 46 vertical levels. We incorporated state-of-the-art parameterization schemes to represent the deep ocean state: the bottom boundary-layer scheme [e.g., *Nakano and Suginohara*, 2002b], the vertical diffusivity schemes [*Gargett*, 1984; *Hasumi and Suginohara*, 1999; *Tsujino et al.*, 2000], and the *Noh* [2004] mixed layer scheme. The major physical parameter values were determined by using an optimization method [*Menemenlis et al.*, 2005] before the assimilation. The adjoint code of the OGCM for the assimilation system was obtained by the Transformation of Algorithms in Fortran (TAF) [*Giering and Kaminski*, 2003].

[16] In the 4D-VAR approach, optimized 4-D data sets are sought by minimizing a cost function. In this study, the cost function consisted of the two summation terms of the squared differences between the fields obtained by observations and analytical data from the model, and the squared differences between the initial values of control

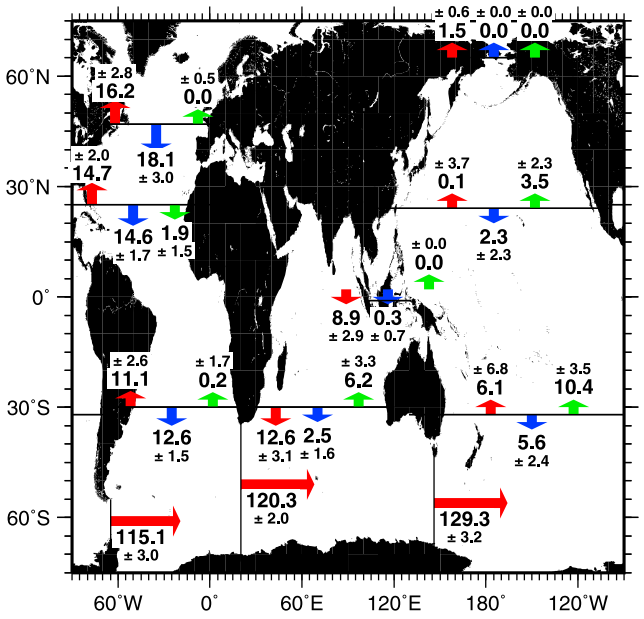

Figure 2. The 40 year mean general circulation used in the reanalysis in this study. Red, blue, and green arrows represent transports ($\times 10^9$ kg s^{-1}) for surface (neutral density $\gamma_n \leq 27.72$ kg m^{-3}), deep (27.72 kg m^{-3} $< \gamma_n \leq$ 28.11 kg m^{-3}), and bottom ($\gamma_n >$ 28.11 kg m^{-3}) layers, respectively. Horizontal red arrows around Antarctica show the barotropic transports (the sum of the transports in the three layers).

variables (initial ocean states and air-sea fluxes) and their guesses from the assimilation system, which is similar to the method used by *Stammer et al.* [2002]. Because they are not well known, error covariance matrices for the observational data and the control variables in the cost function were assumed to be diagonal, and were determined from the temporal changes of the corresponding variables at each grid model point.

[17] The differences between the observations and the model data below the surface (at the surface), which were used for the cost function, were calculated from a monthly (10 daily) mean value of model data and the one obtained from observations in 1° by 1° bins. In addition, we incorporated the differences between 5 year, 10° box mean temperature and salinity fields obtained from observations and the model below 2000 m for the summation term in the cost function to enhance the representation of the deep ocean [*Masuda et al.*, 2010]. The field obtained by the assimilation technique with the cost function is dynamically self-consistent.

[18] We note that using these settings in the cost function does not artificially smooth out short-term variability, which should be revealed by the model, from the reanalysis product, because the assimilation system constrains the model results not with the value in the model at each model time step, but with the bulk value calculated for each range, which is set in the cost function, and the mean differences in the cost function can be reproduced by a short-term change as well as by the constant or long-term mean difference. Although variability in the ocean shorter than a month is also not artificially smoothed out by this method, we used monthly mean data sets for this analysis because the 10 daily mean air-sea flux fields were used in our assimilation system and the variability shorter than a month might not be sufficiently reproduced.

[19] A data assimilation experiment was performed using the Earth Simulator at JAMSTEC to derive an ocean state estimate for the period from 1957 to 2006. We used a 40 year monthly data set, from 1967 to 2006, to avoid the initial error in the data assimilation. The obtained reanalysis field is in broad agreement with recent observations [*Masuda et al.*, 2010]. For example, the representation of the deep velocity profiles near the Wake Island passage was successful, as the revealed velocity field around the passage was similar to the direct velocity measurements using a moored system [*Uchida et al.*, 2007, 2009], and the sea surface flux revealed by the assimilation system also agreed well with that from Japanese Ocean Flux Data Sets [*Kubota et al.*, 2002] based on remote sensing observations, which was similar to a result in a previous study [*Masuda et al.*, 2003].

[20] Furthermore, we compared the ocean general circulation structure in the reanalysis product with the ones estimated from observations [e.g., *Ganachaud and Wunsch*, 2000], as the temperature changes in the deep ocean can be affected by the circulation structure. North Atlantic Deep Water (NADW) forms around 60°N in the Atlantic Ocean, and its southward transport is 13–18 $\times 10^9$ kg s^{-1} in the 40 year mean layer-averaged transports from the reanalysis product (Figure 2). The northward transports in the bottom layer from the Southern Ocean are 0.2 $\times 10^9$ kg s^{-1} in the Atlantic, 6.2 $\times 10^9$ kg s^{-1} in the Indian, and 10.4 $\times 10^9$ kg s^{-1} in the Pacific oceans. These features are consistent with the estimates obtained using the inverse method [*Ganachaud and Wunsch*, 2000], except for the small northward transport in the bottom layer of the Atlantic Ocean (for which we will discuss a possible cause in section 6). We assume that our reanalysis product are realistic enough to use in estimating the uncertainty in HC trends in recent decades, which are probably due to short-term variability.

3. Heat Content Changes in Observation Data

3.1. Horizontal Distribution

[21] The horizontal distribution of the temperature change rate in each box as determined from the comparison between the WHP and the revisits shows a positive temperature change extending over almost all of the global ocean below 3000 m (Figure 3). Larger temperature increases were observed nearer to Antarctica, as was also shown by *Purkey and Johnson* [2010]. The temperature change around the Weddell Sea and the Adelie Coast, where bottom water is formed, was about 0.05–0.08°C decade^{-1} in the layer from 4000 to 5000 m, which corresponds to an additional local surface heat flux of 0.4–0.6 W m^{-2} to account for the temperature changes in this layer (Figure 3b).

[22] In the Pacific Ocean, the temperature increased in most of areas at depths below 4000 m, whereas temperature decreases were observed in some boxes in the layer from 3000 to 4000 m (Figure 3a). Because of the way we divided the Pacific Basin into boxes, we could detect the relatively strong temperature increases along the northward path of

(a) 3000–4000 m

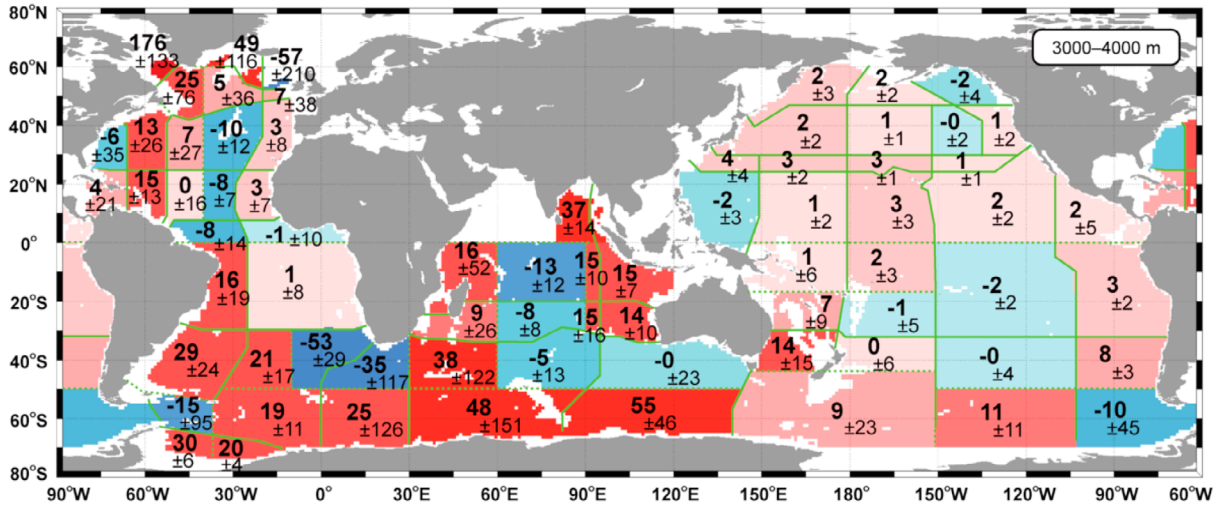

(b) 4000–5000 m

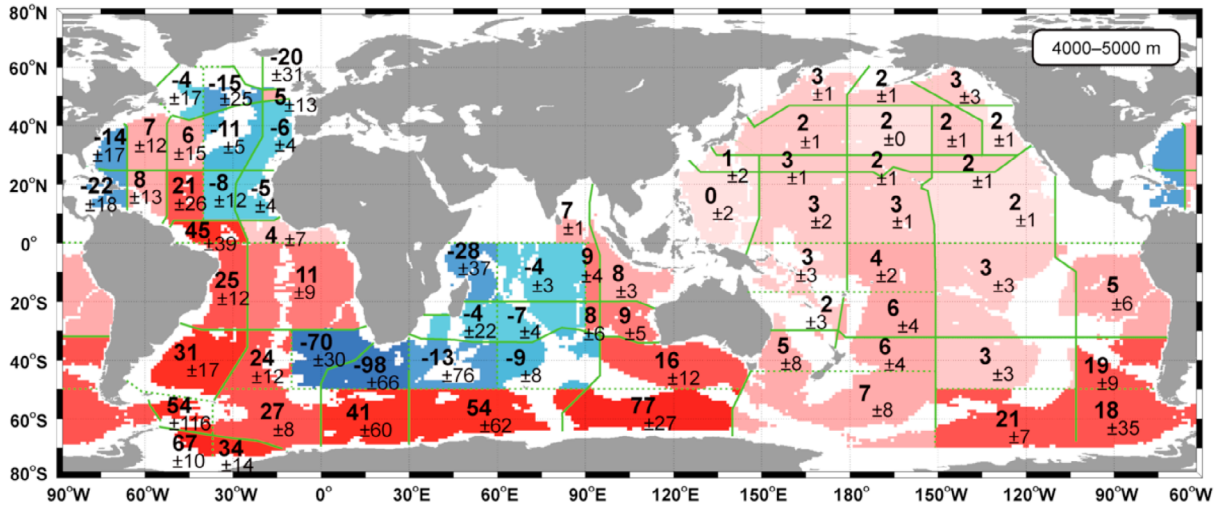

(c) 5000 m–bottom

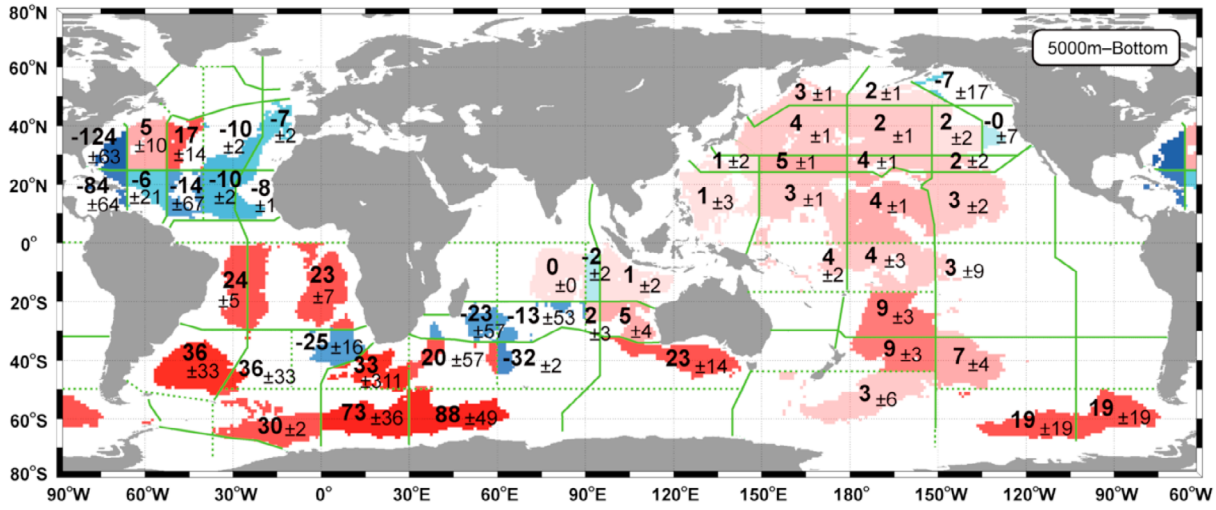

Figure 3. Horizontal distribution of the temperature change rate with 90% confidence intervals ($\times 10^{-3}$ °C decade^{-1}) in the (a) 3000–4000 m, (b) 4000–5000 m, and (c) 5000 m to bottom layers. Red indicates positive change (temperature increase); blue indicates negative change (temperature decrease).

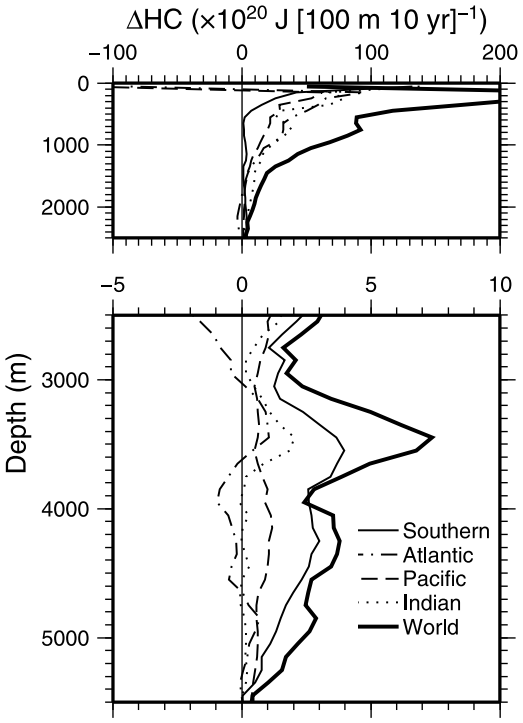

Figure 4. Vertical profile of the heat content (HC) changes in each ocean and in the global ocean. HC changes for the Pacific are the sum of the changes in boxes 1–26, for the Atlantic are the sum of the changes in boxes 27–50, for the Indian are the sum of the changes in boxes 51–63, and for the Southern Ocean are the sum of the changes in boxes 64–73 (see Figure 1).

Circumpolar Deep Water (CDW) in the layer from 4000 to 5000 m in the center of the Pacific (Figure 3b), as was also shown by *Kawano et al.* [2010]. Although the temperature increase in the western part of the southern Atlantic Ocean might have also been affected by the increase around Antarctica, a temperature decrease was observed in the 3000–5000 m layer of the Indian Ocean. As there are fewer observation lines available in the Indian Ocean than in the other oceans, estimates of the temperature changes in the Indian Ocean, particularly in the northwestern part, are less accurate than those in the other areas. Indeed, *Purkey and Johnson* [2010] showed large confidence intervals for HC changes in the Indian Ocean.

[23] In the northern Atlantic Ocean, the largest temperature increases were detected off Greenland, and the temperature increase in the 3000–4000 m layer there was about the same as that around Antarctica (Figure 3a). This strong temperature increase, which reflects the temperature increase along line AR07 (see Figure 1 and Table 1), was due to large interannual variability in the temperature of Denmark Strait Overflow Water (DSOW) reported by previous studies [e.g., *Dickson et al.*, 2002; *Yashayaev*, 2007], as DSOW was observed near the bottom off Greenland, where the bottom depths are typically 3000–4000 m. The long-term freshening in deep water off Greenland after the 1970s [e.g., *Dickson et al.*, 2002; *Curry et al.*, 2003; *Yashayaev*, 2007] was also detected in the layer from 2000 to 3000 m in our analysis (not shown).

3.2. Heat Content Change

[24] Vertical distributions of the global and basin-scale decadal differences in HC from the 1990s to the 2000s were calculated using the temperature change rates (Figure 4), as shown in Figure 3 for the deep layers. The global HC increase in the layer from 0 to 700 m was 10×10^{22} J decade^{-1} (or 7.8×10^{22} J decade^{-1} excluding the Southern Ocean). In the upper layer, the strong seasonal variability and the water mass distribution changes due to gyre shifts, which are mainly due to interannual variability of wind forcing [e.g., *Deser et al.*, 1999; *Joyce et al.*, 2000; *Roemmich et al.*, 2007], cause large uncertainties in estimating HC changes using sparse and nonuniform observations [*Roemmich and Gilson*, 2009]. Although we also could not avoid the large aliasing effect from using the sparse and nonuniform observations in our estimation of the HC changes, the estimated HC increase was not very different from the estimates of about 4–11 $\times 10^{22}$ J decade^{-1} from previous studies [e.g., *Willis et al.*, 2004; *Ishii et al.*, 2006; *Freeland and Gilbert*, 2009; *Levitus et al.*, 2009; *Lyman et al.*, 2010]. This suggests that the method used for estimating HC change can better reproduce the HC changes in the deep ocean, where the seasonal variability should be weaker than in the shallower layers.

[25] A large HC increase was detected around 2500 m (Figure 4). This increase was due primarily to the increases in the Indian and Southern Oceans. The global HC change was minimum around 3000 m and increased below 3000 m, mainly due to the increase in the Southern Ocean. The HC increase below 3000 m was evident in the positive temperature changes in each basin (see Figure 3), and might reflect the influence of property changes in water masses formed around Antarctica, such as Antarctic Bottom Water (AABW) and CDW.

[26] The HC increase below 4000 m in the Pacific Ocean was relatively large, and evident as a broad distribution of positive temperature changes in the bottom layer (Figures 3b and 3c) along the path of CDW. Although the Atlantic and Indian oceans contributed to the global HC increase around 3500 m, the HC increases in these two basins were weak below 4000 m. The weak HC increase below 4000 m in the Atlantic Ocean was mainly due to the small volume of bottom water from Antarctica. Indeed, a strong temperature increase was detected in the southwestern part of the Atlantic Ocean (but over a small area), where bottom water with properties similar to AABW is detected [*Johnson*, 2008]. The small contribution of the Indian Ocean to the global HC increase might be due to the smaller bottom layer volume in the Indian Ocean than in the Pacific Ocean. However, because a deep temperature decrease was detected in the western part of the Indian Ocean, where *Johnson* [2008] reported a large proportion of AABW in the bottom water, and this decrease reduced the overall HC increase in the Indian Ocean, the estimated HC increase in the Indian Ocean might also reflect the aliasing effect resulting from sparse and nonuniform observations.

[27] The total global HC increase below 3000 m (4000 m) was 0.8 (0.4) $\times 10^{22}$ J decade^{-1}. A heat flux of 0.1 (0.07) W m^{-2} would be required through 3000 m (4000 m) to account for this HC increase. The HC increases in the deep layer (below 3000 m) are estimated at 5.0% of the full depth HC

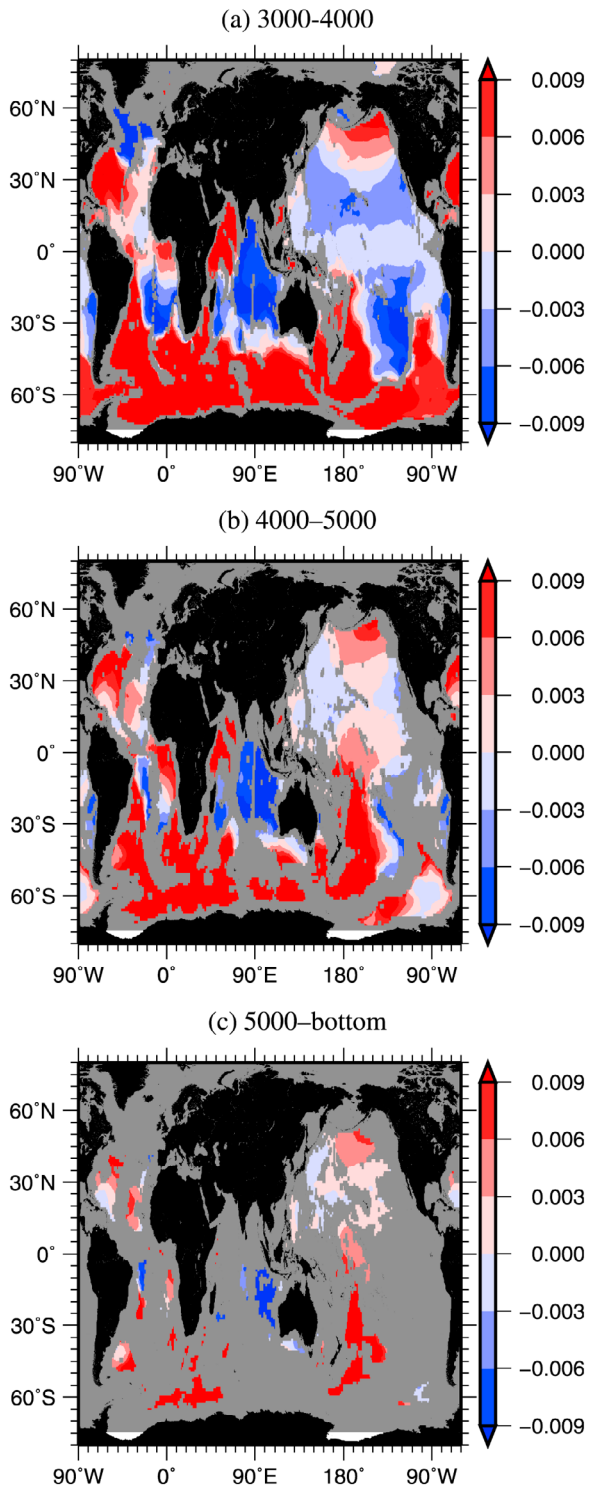

Figure 5. Horizontal distribution of temperature differences in the reanalysis product (°C decade^{-1}) between the periods of 1985–1994 and 1997–2006 (corresponding to the WHP and revisits, respectively) in the (a) 3000–4000 m, (b) 4000–5000 m, and (c) 5000 m to bottom layers. Red indicates positive change (temperature increase); blue indicates negative change (temperature decrease).

changes in the global ocean, 8.7% of changes in the Pacific, 0.4% in the Atlantic, 1.5% in the Indian, and 16.2% of the full depth changes in the Southern Ocean. The proportion of the global ocean changes increase to 8–20% if the HC trends in the shallow layer from previous studies are used; these studies used much more data than in this analysis. Thus, we conclude that the HC changes in the deep ocean cannot be ignored when considering the decadal changes in ocean heat budgets.

4. Heat Content Trend in Reanalysis Product

4.1. Horizontal Distribution

[28] The temperature differences between the two periods of 1985–1994 and 1997–2006 in our reanalysis product (Figure 5) were similar to the ones from observations (Figure 3), although there is a negative offset in the reanalysis product relative to the observations in the 3000–4000 m layer in the North Pacific and below 4000 m in the eastern part of the Indian Ocean. In these areas, it was difficult to detect significant temperature changes by a comparison of two sets of observations along the sections [e.g., *Johnson and Doney*, 2006; *Johnson et al.*, 2007, 2008]. The differences between maps of temperature changes determined from the observations and from the reanalysis product could be caused by the aliasing effect of sparse observations as well as model biases.

[29] The ocean temperature around Antarctica increased from 1967 to 2006 in the reanalysis product, and a time series of decadal mean temperature anomalies shows that the positive anomaly gradually extended to the north (Figure 6). This feature was especially clear in the Pacific Ocean, implying the propagation of the warming signal from south to north. Based on a sensitivity experiment using the same data assimilation system as in the present study, *Masuda et al.* [2010] reported that the warming signal around Antarctica can move into the North Pacific by internal Kelvin and Rossby wave propagation and the warming signal can be caused by buoyancy flux changes around the bottom water formation regions.

[30] As the anomaly pattern for the last decade (Figure 6d) is similar to the temperature differences between WHP and the revisits in the reanalysis product (Figure 5b) and in the observations (Figure 3), it is possible that most of the observational temperature changes are due to long-term variation, and the distribution of the positive HC changes could be caused by the mechanisms reported by *Masuda et al.* [2010], especially in the Pacific Ocean.

[31] In the western part of the South Atlantic Ocean, the anomaly pattern of the last decade (Figure 6d) was slightly different from the temperature changes between WHP and the revisits (Figure 5b), whereas the temperature increase was reproduced (Figures 3 and 5). This increase was reported by comparisons along the sections in a previous study [*Johnson and Doney*, 2006]. This may reflect both the short-time propagation of temperature anomalies, as suggested from the analysis of observational data in the Argentine Basin [*Coles et al.*, 1996], and the modulation of the trend of temperature increase, as *Zenk and Morozov* [2007] reported that the clear long-term temperature increase started from 19 92 after a period of weak temperature increase from 1972 to 1991.

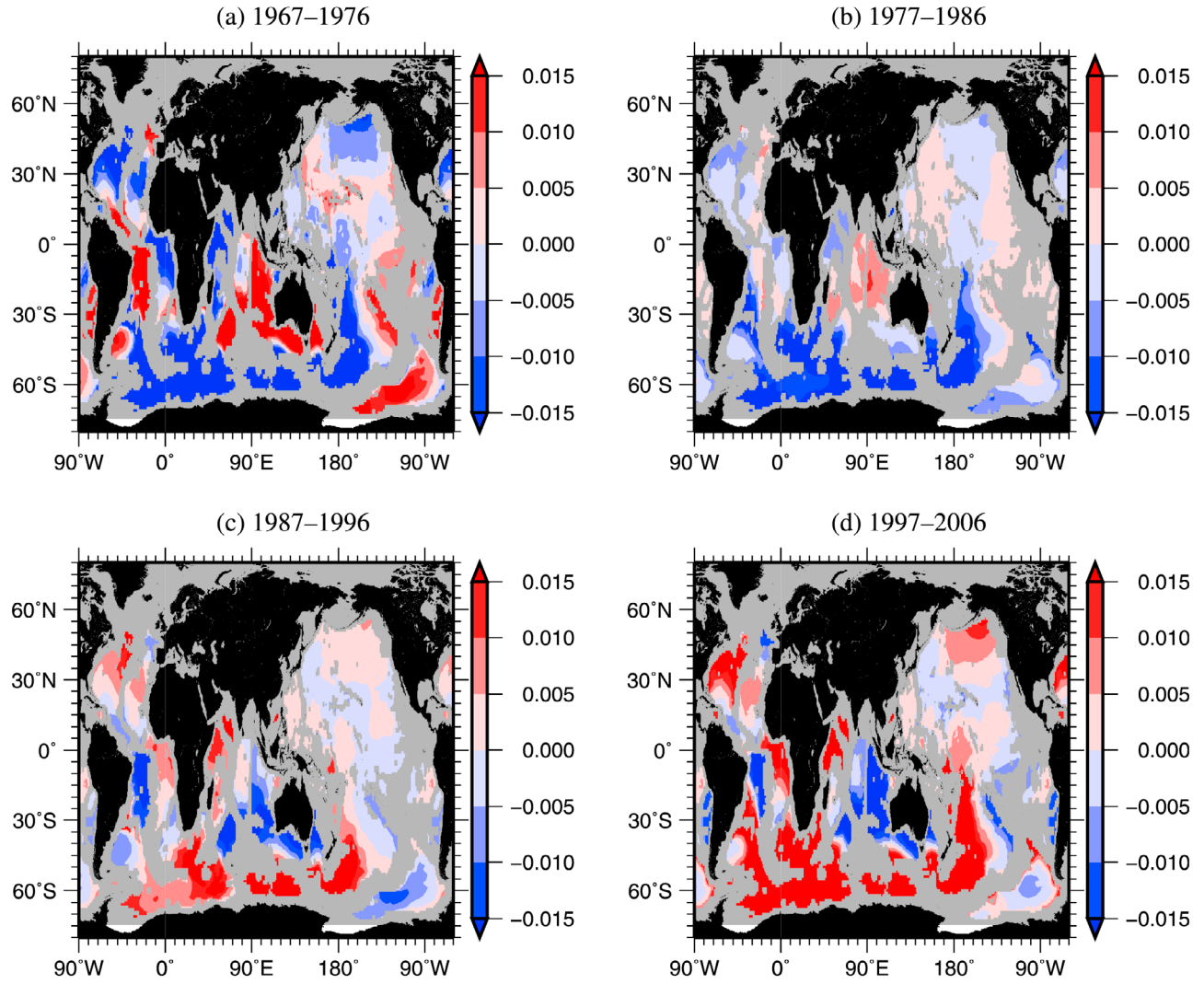

Figure 6. Horizontal distribution of the temperature anomaly (°C) in the layer from 4000 to 5500 m relative to 40 year average temperatures at each grid point. Red and blue indicate positive and negative anomalies, respectively.

4.2. Heat Content Trends and Virtual Observations

[32] Even in the deep ocean the temperature can be affected by local forcing as well as by remote forcing, especially around areas where bottom water is formed, so the estimation of temperature changes by a comparison of two observations cannot avoid the effect of aliasing. We evaluated the validity of estimating HC changes from observational data using our reanalysis product. Given that our reanalysis product reproduces variability in the deep ocean, we obtained probability density functions for HC estimates by using all possible combinations of "virtual observations", in our reanalysis product, that might have been carried out along 25 observation lines (red lines in Figure 1) during the two periods of 1985–1994 (120 months for WHP) and 1997–2006 (120 months for the revisits). As the total number of possible combinations is extremely large ($120^{25} \times 120^{25}$), even assuming an observation line was occupied within a month, we estimated the probability density functions from 10,000 random samplings of the all the possible combinations in the monthly reanalysis product.

[33] Note that we here used the probability density functions for estimates of the uncertainties, as it was more accurate than confidence intervals based on the *t* test, which assumes the normal distribution for sample means. Indeed, the probability density functions were different from the normal distribution at a statistically significant level (not shown).

[34] For the random sampling, we determined the months during WHP and the revisits when observation lines were occupied, using the uniform pseudorandom number generator developed by *Matsumoto and Nishimura* [1998], and obtained the set of virtual WHP and revisit observations. The HC changes were calculated using the set thus obtained by the same method as used with the actual observations, and we obtained 99% confidence intervals for the HC changes from the probability density function estimated from the 10,000 virtual observations. Because results from 1000 virtual observations (not shown) were similar to results from the 10,000 virtual observations, we believe the 10,000 virtual observations are enough to estimate the probability

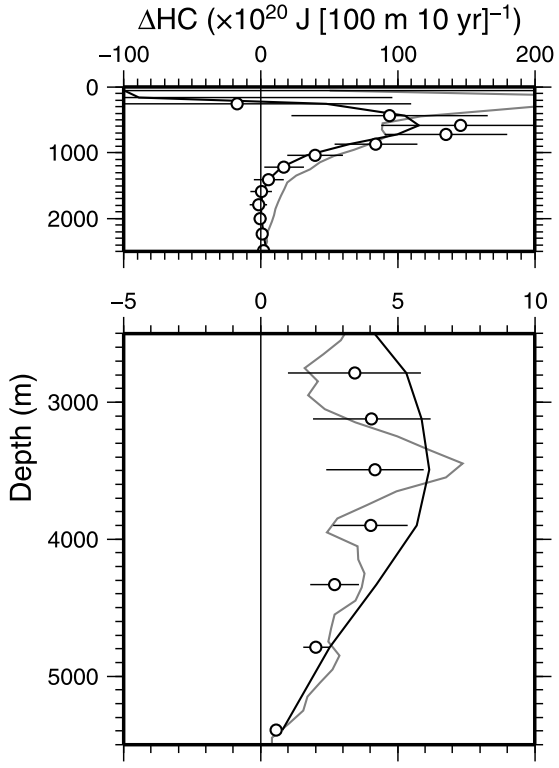

Figure 7. Vertical profiles of decadal trends of HC change in the world ocean from 1985 to 2006 in the assimilation data sets. Black curve indicates the HC trend estimated with the full grid assimilation data. Black circles indicate the mean HC changes from 10,000 virtual observations using the same method as for the observational estimate. The black bars show 99% confidence intervals of the estimates from the virtual observations. The gray curve is the profile of HC changes estimated from the actual observations (same as the thick black curve in Figure 4).

density function. In the following paragraphs, we show HC trends estimated on the basis of the full grid data in the reanalysis product and HC changes estimated from virtual observations using the same method as for the observational estimate. Note that the HC trends estimated from the full reanalysis product are not necessarily within the confidence intervals for the HC changes determined from the virtual observations because the simple method using the box-average temperature change rates and the spatially nonuniform and sparse distribution of the observation lines can result in larger biases.

[35] The vertical profile of the global HC trend based on the full reanalysis product (black curve in Figure 7) is similar to the HC changes estimated from the virtual observations (black circles in Figure 7), although there are some biases in the estimates from full reanalysis product compared to those from virtual observations, especially below 3000 m where the estimates are strongly affected by the lack of data from the northwestern part of the Indian Ocean from the virtual observations (white area in the Indian Ocean in Figure 3). This overall agreement suggests that the available observational system can capture the true decadal HC trend, although there are large uncertainties, especially in the upper 1000 m, which are visible in the 99% confidence intervals (Figure 7).

[36] The global HC trend was also consistent with that estimated from observations (gray curve in Figure 7) except in the upper 1000 m. The HC trend (95% confidence interval estimated using estimated degrees of freedom taking into account temporal decorrelation lengths of 2–3 years (not shown)) for the upper 800 m using full reanalysis product is +3.4 (±2.0) × 10^{22} J decade^{-1} for 1985–2006 (+6.0 [±3.2] × 10^{22} J decade^{-1} for the typical analysis period of 1993–2006 in previous studies), and this value is closer to the estimates from previous studies [e.g., *Ishii and Kimoto*, 2009] than the observational estimate in the present study. However, HC change in the upper 800 m from the virtual observations is 1.2 × 10^{22} J decade^{-1} for 1985–2006, and the range of the 99% confidence interval is quite large (Figure 7). This shows that HC change estimates from spatially and temporally nonuniform observations have substantially large uncertainties, as pointed out by a previous study [*Roemmich and Gilson*, 2009], although the HC changes in the upper 800 m from the real observations was not very different from the estimates in previous studies as shown in section 4.1.

[37] The HC change estimated below 3000 m from the virtual observations is +0.7 × 10^{22} J decade^{-1}, with a 99% confidence interval of 0.4–1.0 × 10^{22} J decade^{-1}, similar to the values based on observations. This value (95% confidence interval) is slightly less than the trend of +1.0 (±0.1) × 10^{22} J decade^{-1} estimated from the full reanalysis product. This difference could be caused by a bias in HC change estimation using a spatially sparse system of real observations (including the lack of observations in the northwestern part of the Indian Ocean) as well as the difference between the HC change fields in the real ocean and in our reanalysis product. The 99% confidence intervals for the estimates using the virtual observations show that the positive HC trend below 3000 m (Figure 7) could be detected by the WHP and revisit observation system.

[38] This reanalysis shows that the HC trend below 3000 m from full reanalysis product is about 30% (18%) of that in the upper 800 m for 1985–2006 (for 1993–2006). This result supports the result from the observational analysis in section 4.1 that HC variability in the deep ocean cannot be ignored when estimating the heat balance in the global ocean, although the proportion is larger in the reanalysis product than in the observational analysis.

[39] We determined the HC trends for each ocean from our reanalysis product (Figure 8). There are large differences between the trends from the reanalysis and the observational estimates in the upper 2000 m. In the layer from 0 to 1000 m in the Indian Ocean, the difference is greater than 2 × 10^{22} J decade^{-1}. This large difference is the primary reason for the difference between the reanalysis and observation estimates in Figure 7. The large difference is mainly due to the sparseness of the observations in the Indian Ocean, which causes both large uncertainties in the observational estimates and lower reproducibility of the reanalysis product.

[40] The increasing trend below 3000 m was the largest in the Southern Ocean, and the HC increases around 4000 m in the Pacific Ocean and around 3000 m in the Atlantic and Indian oceans contributed to the global HC increase below 3000 m. This feature is similar to that in the observational

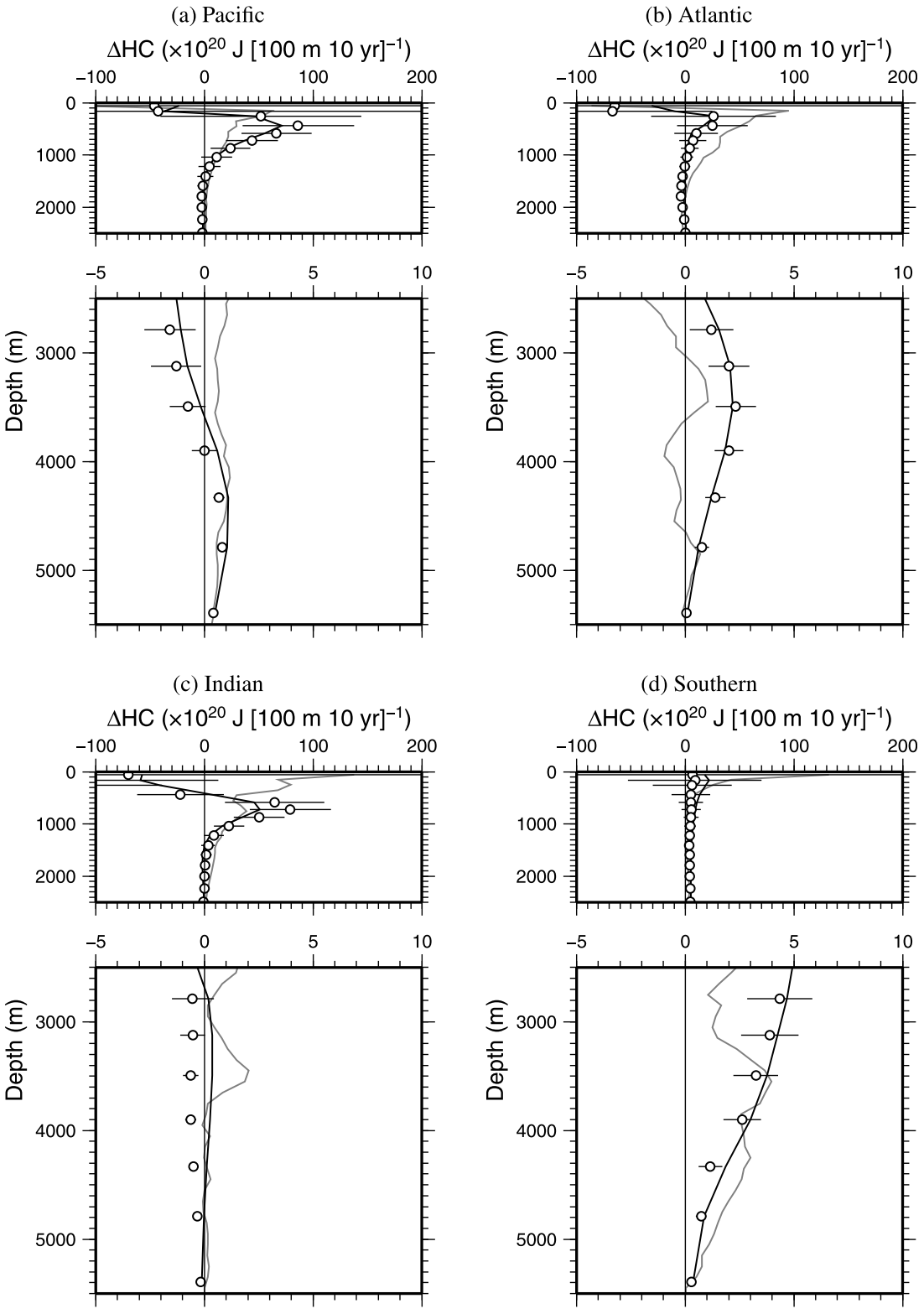

Figure 8. Vertical profiles of decadal trends in HC changes from 1985 to 2006 in the reanalysis for each ocean. Curves and symbols are the same as in Figure 7.

estimates described in section 3.2. The vertical profiles of HC trends were similar to the changes estimated from the virtual observations, except in the Indian Ocean. This suggests that the HC changes in each ocean can be evaluated using the available observations.

[41] In the Pacific, the total HC trend below 3000 m (4000 m) in the reanalysis was estimated at 0.1 (0.1) × 10^{22} J decade^{-1}, which corresponds to an additional heat flux of 0.03 (0.05) W m^{-2} at the depth of 3000 m (4000 m). The changes estimated from observations are similar to the

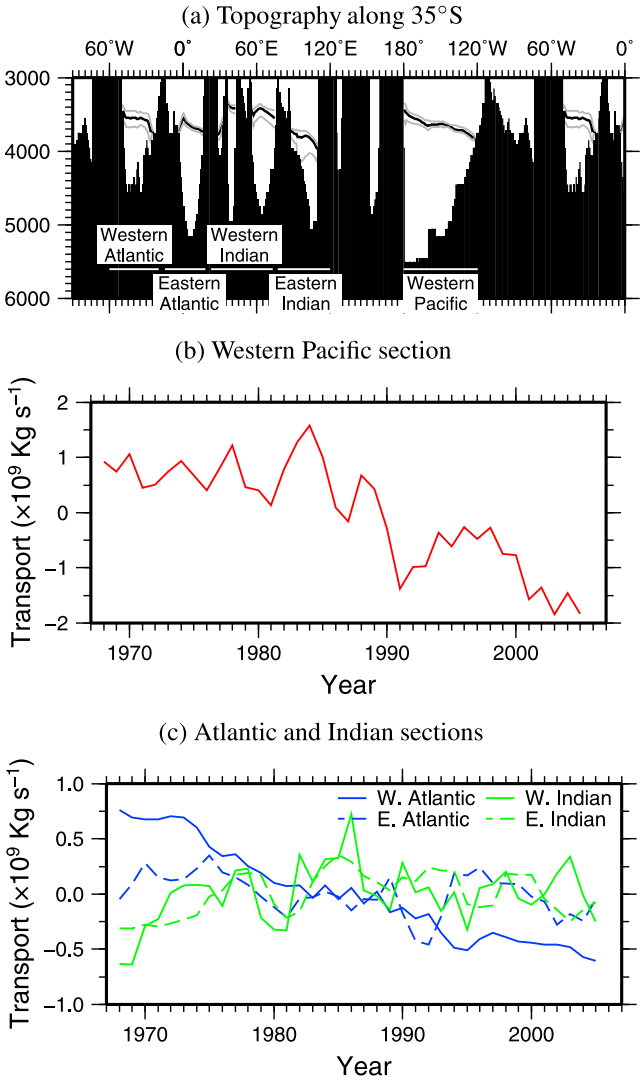

Figure 9. Northward transport anomalies for the major bottom water paths at 35°S. (a) Bottom topography and neutral density γ_n surface near the depth of 3500 m used to calculate the transports. Black contours show the 40 year mean neutral density surfaces of γ_n = 28.18 kg m^{-3} for the Atlantic and the western Indian sections and γ_n = 28.16 kg m^{-3} for the eastern Indian and the western Pacific sections. Gray contours are the minimum and maximum depths of the neutral density surfaces in the monthly reanalysis product, which show that the bottom waters below the selected neutral densities did not overflow into the other basins. Horizontal white bars show the longitudinal ranges used for transport calculations. (b) The 3 year running mean northward transport anomaly (from the 40 year mean) for the western Pacific section. (c) Same as Figure 9b but for the Atlantic and Indian sections. The blue solid and dashed curves show the transport anomalies of the bottom water for the western and eastern Atlantic sections, respectively. The green solid and dashed curves show the same for the western and eastern Indian sections, respectively.

ones from the reanalysis in the layer below 4000 m, whereas the HC changes in the upper 3000 m estimated from the reanalysis product differ from those from observations, and the confidence intervals for the estimates from virtual observations above 3000 m become wider than for those near the bottom (Figure 8a).

[42] In the Atlantic Ocean, the total HC trend below 3000 m (4000 m) in the reanalysis is 0.3 (0.09) × 10^{22} J decade^{-1}, which corresponds to an additional heat flux of 0.18 (0.07) W m^{-2} at 3000 m (4000 m). Although the vertical profile of HC trends estimated from the reanalysis product in the Atlantic has a maximum around 3000 m, which is similar to the HC changes estimated from observations, there is a positive offset in the HC trends for the reanalysis product from the observational estimates (Figure 8b). The small positive offset might be due to model biases.

[43] In the Indian Ocean, the total HC trend below 3000 m (4000 m) in the reanalysis has a low value of 0.03 (0.00) × 10^{22} J decade^{-1}, corresponding to an additional heat flux of 0.02 (0.00) W m^{-2} at 3000 m (4000 m). There are large differences between the estimates based on full reanalysis product and virtual observations (Figure 8c). This implies that the available observations were too sparse to describe the HC changes in the Indian Ocean, whereas the trend based on the full reanalysis product is similar to the HC changes estimated from observations.

[44] In the Southern Ocean, the total HC trend below 3000 m (4000 m) in the reanalysis is large at 0.56 (0.14) × 10^{22} J decade^{-1}, which corresponds to an additional heat flux of 0.5 (0.2) W m^{-2} at 3000 m (4000 m). The confidence intervals for the estimates from virtual observations in the deep ocean were the widest among the all oceans (Figure 7), which were caused by large variability of front locations and bottom water properties around Antarctica.

4.3. Bottom Water Transport Variability

[45] The bottom layer HC changes determined in each basin in the reanalysis product (Figures 6 and 8) are related to the changes in northward transport from Antarctica, as previously shown in the Pacific Ocean [*Masuda et al.*, 2010] because AABW is fed into the global bottom layers [*Johnson*, 2008] by the meridional overturning circulation [e.g., *Lumpkin and Speer*, 2007]. As shown by *Masuda et al.* [2010], the northward transport of bottom water below the neutral density surface near 3500 m depth across the western Pacific section (Figure 9a) decreased substantially in recent decades (Table 2 and Figure 9b) and this decrease has caused the widespread warming in the bottom layer of the Pacific (Figure 6).

Table 2. Trend in the Bottom Water Northward Transport (× 10^9 kg s^{-1} decade^{-1})[a]

Section	Trend (95% Confidence Interval)
West Pacific	−0.71 (±0.23)
West Atlantic	−0.36 (±0.06)
East Atlantic	−0.07 (±0.07)
West Indian	+0.12 (±0.11)
East Indian	+0.05 (±0.09)

[a]See Figures 9b and 9c. The 95% confidence intervals were calculated using temporal decorrelation lengths of about 3 years, which were estimated at each section.

Table 3. Effect of Temperature T and Salinity S Changes Below 3000 m on the Steric Height Changes (mm yr^{-1})

Data Sets	Effects	Ocean Basin				
		Pacific	Atlantic	Indian	Southern	Global
Observations	T	0.025	0.017	−0.002	0.065	0.105
	S	−0.013	0.010	0.005	−0.012	−0.010
	Total	0.013	0.027	0.003	0.053	0.095
Reanalysis	T	0.018	0.039	0.003	0.061	0.121
	S	0.022	−0.019	−0.001	0.007	0.009
	Total	0.040	0.020	0.002	0.068	0.130

[46] There are two major paths of northward bottom water transport in the Atlantic (Figure 9a). The northward transport across the western Atlantic section also decreased (Figure 9c) and this slight decrease (Table 2) could have resulted in the temperature increase along the western side of the southern Atlantic (Figure 6). There is no substantial trend in northward transport across the eastern Atlantic section (Table 2). The large variability of the northward transport (Figure 9c) might be the cause of the differences in temperature change rates between the reanalysis (Figure 6) and observational estimates (Figure 3) along the west coast of southern Africa, while the basin north of the section is small and the temperature changes there did not strongly contribute to the HC changes in the Atlantic Ocean. However, as the northward transport of bottom water in the South Atlantic in our reanalysis product was smaller than the estimate from observations [e.g., *Ganachaud and Wunsch*, 2000] (Figure 2), the relationship between the transport variability and the temperature changes in the real ocean is not conclusive. The difference between transports in our reanalysis product and the observations are discussed in section 6.

[47] In the Indian Ocean, the bottom water follows two major paths northward (Figure 9a). The 40 year mean northward transports in the bottom layers across the western and eastern sections were 1.6 and 2.3 × 10^9 kg s^{-1}, respectively. This estimate for the eastern section is similar to that for AABW into the Perth Basin estimated from 1 year moored current meter data [*Sloyan*, 2006], whereas *Sloyan and Rintoul* [2001] estimated a 6 Sv northward transport of AABW along 32°S using an inverse method and data from the hydrographic sections around Antarctica. Furthermore, the 40 year mean transport below the neutral surface of 28.0 kg m^{-3} (about 2000 m depth; not shown) on the eastern side of the Indian Ocean in our reanalysis product was 6.7 × 10^9 kg s^{-1}; within the wide range of estimates from the observations of 1–7 Sv [e.g., *Toole and Warren*, 1993; *Ganachaud and Wunsch*, 2000; *Sloyan and Rintoul*, 2001].

[48] In a section corresponding to the western section of the Indian Ocean in this study without the Madagascar Basin, which is located between 20°E and 45°E (Figure 9a), the northward transport in the deep layer was estimated to be 4–6 Sv using hydrographic observations [e.g., *Toole and Warren*, 1993; *Ganachaud et al.*, 2000; *Sloyan and Rintoul*, 2001]. This range of estimates from the observations is higher than the estimate in this study, although *Ganachaud et al.* [2000] showed a large uncertainty of ±8 Sv for their estimate. This difference may be due to the complicated topography of the Southwest Indian Ridge, located from 40°S, 50°E to 25°S, 65°E, which has many deep, narrow paths that are difficult to resolve in our coarse resolution model, as well as to the large uncertainty of the observational estimate.

[49] Although there are no substantial 40 year trends in the western and eastern Indian sections (Table 2), the transports across the western Indian section increased from 1970 to 1985, decreased from 1985 to 1995, and then increased again after 1995 (Figure 9c). The increase after 1995 could be the cause of the temperature decrease in the most recent decade (Figure 6d). Although the interannual variability of the transport across the eastern Indian section is similar to that across the western Indian section (Figure 9c), the decadal trend of northward transport across the eastern Indian section is smaller than the one across the western section. However, more observational data are needed to describe the relationship between temperature and bottom water transport in the Indian Ocean, as the variability of northward transport there is relatively large and the topography is complicated.

5. Steric Height Change due to Deep Ocean Changes

[50] The HC changes described in section 3.2 can contribute to sea level changes. Changes in sea level were calculated using the following equations:

$$\eta_t = \frac{1}{A}\int_{bottom}^{3000} \frac{\rho_o - \rho(S_o, T, p)}{\rho_o} a(z)dz,$$
$$\eta_s = \frac{1}{A}\int_{bottom}^{3000} \frac{\rho_o - \rho(S, T_o, p)}{\rho_o} a(z)dz \quad (1)$$

where η_t and η_s are the thermosteric and halosteric changes, respectively; A and $a(z)$ are the global sea surface area and the area for each depth z, respectively; and ρ is the density, which is a function of salinity (S), temperature (T), and pressure (p) for each depth. S_o, T_o, and ρ_o are the reference salinity, temperature, and density, respectively, and are the mean salinity, temperature, and density of WHP and revisit observations for the observational estimate, and the 40 year mean (1967–2006) for the reanalysis product estimate. For the reanalysis product, we used depth in stead of pressure for calculating density in this analysis.

[51] The contributions of the HC and salinity changes below 3000 m to the global sea level change are summarized in Table 3. In these estimates, the combined contribution to total decadal sea level rise was 0.095 mm yr^{-1} based on observations and 0.130 mm yr^{-1} from our reanalysis product. The bottom water warming in the Pacific, Atlantic, and Southern oceans strongly affected the global sea level rise in both the observation and reanalysis product. The halosteric changes were much smaller than the thermosteric changes in both the observation and reanalysis product, and halosteric changes differed between the observation and reanalysis product (Table 3).

[52] Local steric changes were calculated using equations similar to equation (1), but the total area (A) was set to the area at 3000 m depth for each box.

[53] The halosteric contribution to local steric changes can be important because, in some areas, the magnitudes of the halosteric and thermosteric changes were similar (Figure 10). As the halosteric contributions were opposite to the ther-

(a) Temperature

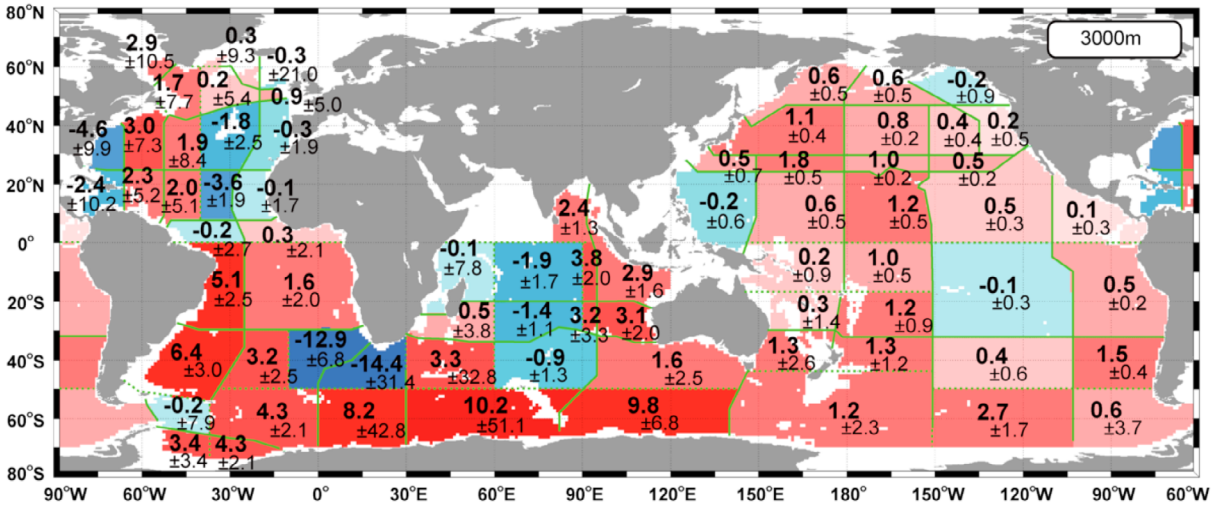

(b) Salinity

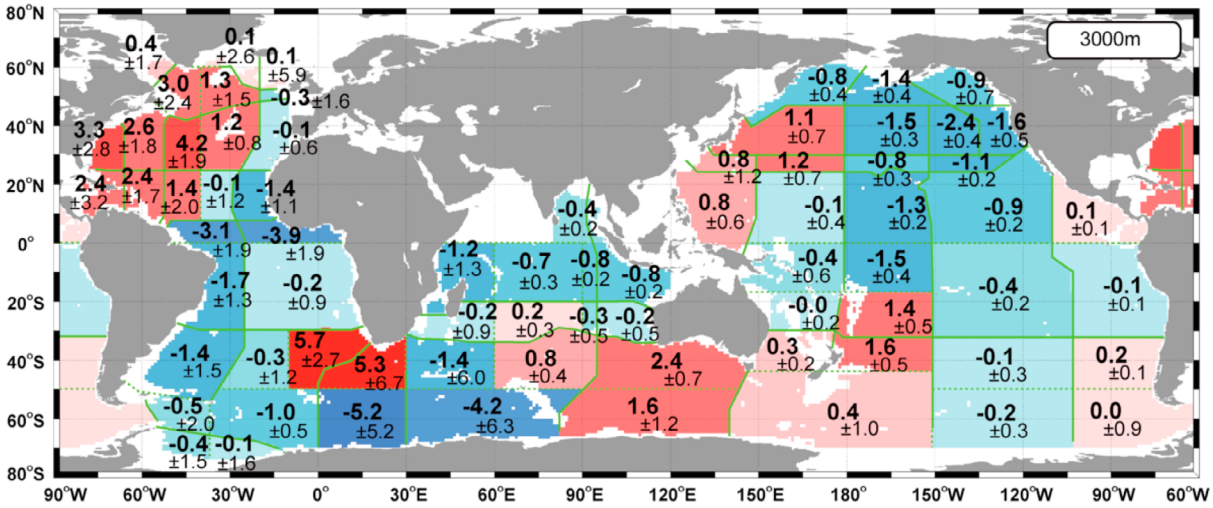

(c) Total

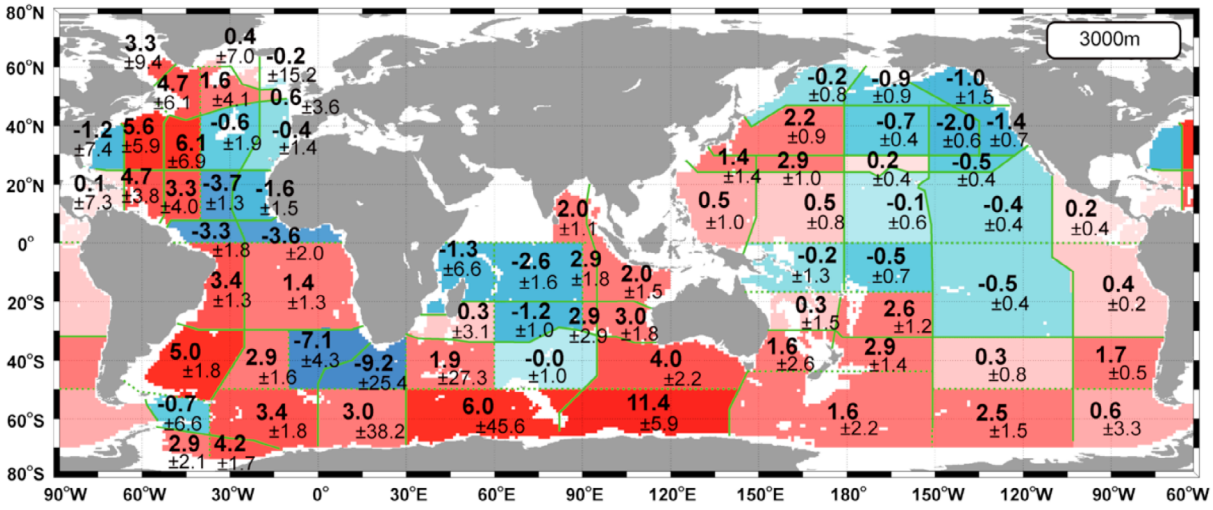

Figure 10. Horizontal distribution of the influence on the steric height (mm decade^{-1}) with 90% confidence intervals above each box from changes below 3000 m in (a) temperature, (b) salinity, and (c) density (temperature and salinity combined).

mosteric changes in the North Pacific, South Atlantic, and the area from 90°W–90°E in the Southern Ocean, the total steric height increase in these areas was less than the thermosteric height increase. However, the measurement accuracy of salinity (about 0.003), which was estimated from the comparison of salinity values at the crossover points of the WHP sections [*Johnson et al.*, 2001], can create errors about 6 times larger than that of temperature in the calculation of density, and it was difficult to detect the halosteric changes described above when measurement errors were considered.

[54] In contrast, near the Adelie Coast of Antarctica and in the western South Pacific, the halosteric and thermosteric changes were both positive, and the halosteric changes were detectable. The positive steric increase around the Adelie Coast was similar to the result reported by *Johnson et al.* [2008] through careful comparison of hydrographic observations along I08S. As saltier and colder bottom water is formed through brine rejection associated with sea ice formation near the Adelie Coast, the positive contribution to sea level change might reflect the reduction in bottom water formation, as shown in previous studies through comparisons of hydrographic observations [e.g., *Katsumata and Fukasawa*, 2010].

6. Discussion

[55] In this study, we mapped the decadal temperature changes and estimated the decadal HC changes in the deep ocean. There have been many studies of HC variability in the shallower ocean layers. For example, *Levitus et al.* [2005] showed that the HC in the upper 3000 m of the global ocean increased by 14.5×10^{22} J from 1955 to 1998. *Ishii and Kimoto* [2009] estimated an HC increase of about 6.0×10^{22} J decade^{-1} from 1993 to 2003. These estimates were larger than the estimates from the observational data in the present study. Although the increase of 0.8×10^{22} J decade^{-1} below 3000 m was only about 5% of the HC increase from observational data in the upper layers, this proportion increases in comparison with the values from previous studies. Because the observational data used in this study were sparse and nonuniform, it was not possible to avoid the aliasing effect of the strong seasonal HC variability in the shallow layer. The HC changes below 3000 m in this study were 8–20% of those in the upper layer (typically the upper 700 m) in previous studies [e.g., *Willis et al.*, 2004; *Ishii and Kimoto*, 2009]. This suggests that the HC changes below 3000 m and around Antarctica cannot be neglected in the precise estimation of HC changes in the global ocean.

[56] Our estimated values for the HC change, and the demonstrated importance of the HC change around Antarctica, agree well with the results of *Purkey and Johnson* [2010]. Our results extend theirs by showing the detailed distribution of temperature changes in the deep ocean. Although the uncertainties of the subbasin-scale temperature and steric height changes were large, the changes were still significant in some boxes, such as below 5000 m, south of Australia, and in the center of North Pacific (Figures 3 and 10). Furthermore, we show the uncertainty of the estimation, mainly due to temporal variability, by using the 4D-VAR data assimilation product. *Purkey and Johnson* [2010] estimated HC changes and showed 95% confidence intervals using degrees of freedom explicitly taking into account spatial decorrelation length, and their confidence intervals could include some temporal variability from using all observations, which were carried out in the large basins on different dates. Although their estimation was based on one of the best available methods for estimating the real ocean HC changes from only the observations, and was free from model biases, which are included in our analysis, it is difficult to evaluate the uncertainty due to temporal variability in their results directly because surveys were carried out only twice for most WHP sections. Assuming that our 4D-VAR data sufficiently revealed the temporal variability caused by local and remote forcing changes, our results support the HC increases shown by *Purkey and Johnson* [2010] even explicitly taking into account temporal variability.

[57] Note that the confidence intervals for the global HC changes in the deep ocean in this study are slightly narrower than those shown by *Purkey and Johnson* [2010] suggesting their confidence interval is more conservative than ours. This implies that their decorrelation length of 160 km was probably an overestimate, while the probability density functions in our reanalysis product might be different from those in the real ocean.

[58] Furthermore, our reanalysis product reproduces the positive temperature anomaly spreading throughout the Pacific from 1967 to 2006. This temperature anomaly propagated through internal Kelvin and Rossby waves, and the HC changes below 4000 m observed in recent decades might reflect the reduction in bottom water formation near the Adelie Coast, attributed to a decrease in the heat flux from the ocean to the atmosphere [*Masuda et al.*, 2010]. The recent ocean freshening reported by previous studies [e.g., *Aoki et al.*, 2005; *Rintoul*, 2007] near the Adelie Coast, which is the source region for the bottom water, is consistent with the reduced bottom water transport in our reanalysis product.

[59] We estimated the contribution of both temperature and salinity changes in the deep ocean to sea level rise. The thermosteric contributions in the observation and the reanalysis product were similar to the results of *Purkey and Johnson* [2010], and the halosteric contributions were small. However, the local halosteric contributions to sea level rise were not negligible, as pointed out by *Antonov et al.* [2002] for the shallower layers. The observation data showed that the halosteric contribution was of the opposite sign to the thermosteric contribution throughout most of the Pacific (Figure 10), and the total steric height change in the Pacific was therefore smaller than the contribution estimated using only temperature changes, although the halosteric effects were not conclusive because of the relatively large uncertainty in the salinity measurements. In contrast, substantial freshening has been detected along some sections in the deep ocean [e.g., *Johnson et al.*, 2008; *Katsumata and Fukasawa*, 2010] and this freshening can add to the thermosteric sea level rise.

[60] Transport variability might be related to the HC changes in the deep ocean, as shown in the Pacific Ocean (Figure 9). The temperature increases on the western side of the South Atlantic also seem to correspond to the transport decrease in the deep ocean. However, in our reanalysis product, the northward transport in the bottom layer across

30°S in the South Atlantic was much smaller than the value of 6–7 Sv estimated from observations [*Hogg et al.*, 1999]. One of the causes of this reduced transport is slightly less dense bottom water in our reanalysis product than in the observations. The northward transport below the neutral density surface of 28.12 kg m^{-3} was estimated to be a larger value of about 3 Sv, which is similar to an estimate made using a method similar to our reanalysis [*Wang et al.*, 2010].

[61] The estimate of bottom water transport may be sensitive to the setting of the upper boundary surface because of the large vertical cell in the deep layers of our reanalysis model (about 3000–5000 m). Another cause of the small northward transport is the low horizontal resolution of our reanalysis model, which cannot reproduce the narrow paths of the bottom water in the South Atlantic. This limited reproducibility can result in the differences between the temperature changes in our reanalysis and the real ocean, whereas the decadal temperature difference field in the deep layer of the South Atlantic in our reanalysis product (Figure 5) is similar to the one from observations (Figure 3). This type of difference between the reanalysis product and observed flow occurs in the western section of the Indian Ocean, where there is a ridge with many narrow paths and the northward transport below 2000 m along the ridge was estimated to be about 6 Sv [*Warren*, 1978].

[62] On the eastern side of the South Atlantic, there was little influence from AABW in the northern section (north of 30°S; Angola Basin), and the influence of AABW was limited along the southwestern coast of Africa (Cape Basin), as shown by *Johnson* [2008]. Although the relatively large interannual variability of the transport across the eastern section of the South Atlantic (Figure 9) might be related to the large temperature variability in the region north of the section, both the bottom water volume north of the section and the mean northward transport across the section were small.

[63] We used the monthly reanalysis product to obtain the confidence intervals for our estimates. The confidence intervals might be slightly underestimated from ignoring the shorter-term temperature variability (e.g., daily), although the short-term variability is considered to be small. The coarse resolution model used in this study could not explicitly reproduce the short-term variability; high-resolution model experiments are needed to account for this short-term variability.

[64] Although our 4D-VAR data assimilation product well reproduced the observed temperature trends and showed that it is possible to evaluate the decadal HC changes using the WHP and revisit observation system, there were relatively large differences in results for depths of 1000–2500 m (see Figure 7). This difference was caused mainly by the results from the Indian and Pacific oceans, where the performance of the assimilation model was limited due to sparse data. In the bottom layer, our reanalysis product did not completely reproduce the detailed structure of the bottom water flow reported from observations, which may be due to the coarse resolution in our assimilation system (e.g., with the rough bottom topography and without reproducing eddies explicitly) and can affect the ability to reproduce the temperature changes there. Thus, although the negative bias of the HC trend determined from full reanalysis product compared to the estimate from the virtual observations was mainly due to the spatially nonuniform observations, it is not conclusive whether the HC changes estimated from real observations include a similar negative bias relative to the trend in the real ocean.

[65] Furthermore, geothermal heating effects were not explicitly included in our assimilation, and *Fukasawa et al.* [2004] suggested that geothermal heating could contribute to warming of the bottom water along the 47°N section in the North Pacific Ocean, assuming that the bottom water circulation has slowed in recent decades. A slowing of basin-scale bottom water circulation, through a mechanism described by *Masuda et al.* [2010], also plays an important role in bottom water warming even if geothermal heating cannot be ignored in the heat balance of bottom water. However, the effect of geothermal heating might add uncertainty to the estimated deep ocean changes. More observational studies and comparisons with model data are needed for the precise estimation and evaluation of deep ocean HC changes.

[66] **Acknowledgments.** We extend our thanks and deep appreciation to the late Ikuo Kaneko for his contribution to the organization of this study. We thank all participants who collected and processed the WOCE and revisit data. The comments from anonymous reviewers were useful for improving the manuscript.

References

Antonov, J. I., S. Levitus, and T. P. Boyer (2002), Steric sea level variations during 1957–1994: Importance of salinity, *J. Geophys. Res.*, *107*(C12), 8013, doi:10.1029/2001JC000964.

Aoki, S., S. R. Rintoul, S. Ushio, S. Watanabe, and N. L. Bindoff (2005), Freshening of the Adélie Land Bottom Water near 140°E, *Geophys. Res. Lett.*, *32*, L23601, doi:10.1029/2005GL024246.

Bindoff, N. L., et al. (2007), Observations: Oceanic climate change and sea level, in *Climate Change 2007: The Physical Science Basis: Working Group I Contribution to the Fourth Assessment Report of the Intergovernmental Panel on Climate Change*, edited by S. Solomon et al., pp. 385–432, chap. 5, Cambridge Univ. Press, New York.

Coles, V. J., M. S. McCartney, D. B. Olson, and W. J. Smethie Jr. (1996), Changes in Antarctic Bottom Water properties in the western South Atlantic in the late 1980s, *J. Geophys. Res.*, *101*, 8957–8970.

Curry, R., B. Dickson, and I. Yashayaev (2003), A change in the freshwater balance of the Atlantic Ocean over the past four decades, *Nature*, *426*, 826–829, doi:10.1038/nature02206.

Deser, C., M. A. Alexander, and M. S. Timlin (1999), Evidence for a wind-driven intensification of the Kuroshio Current Extension from the 1970s to the 1980s, *J. Clim.*, *12*, 1697–1706.

Dickson, B., I. Yashayaev, J. Meincke, B. Turrell, S. Dye, and J. Holfort (2002), Rapid freshening of the deep North Atlantic Ocean over the past four decades, *Nature*, *416*, 832–837, doi:10.1038/416832.

Domingues, C. M., J. A. Church, N. J. White, J. G. Gleckler, S. E. Wijffles, P. M. Baker, and J. R. Dunn (2008), Improved estimates of upper-ocean warming and multi-decadal sea-level rise, *Nature*, *453*, 1090–1093, doi:10.1038/nature07080.

Douglass, D. H., and R. S. Knox (2009), Ocean heat content and Earth's radiation imbalance, *Phys. Lett. A*, *373*(36), 3296–3300.

Freeland, H. J., and D. Gilbert (2009), Estimate of the steric contribution to global sea level rise from a comparison of the WOCE one-time survey with 2006–2008 Argo observations, *Atmos. Ocean*, *47*(4), 292–298, doi:10.3137/OC312.2009.

Fukasawa, M., H. Freeland, R. Perkin, T. Watanabe, H. Uchida, and A. Nishina (2004), Bottom water warming in the North Pacific ocean, *Nature*, *427*, 825–827, doi:10.1038/nature02337.

Ganachaud, A., and C. Wunsch (2000), Improved estimates of global ocean circulation, heat transport and mixing from hydrographic data, *Nature*, *408*, 453–457.

Ganachaud, A., C. Wunsch, J. Marotzke, and J. Toole (2000), Meridional overturning and large-scale circulation of the Indian Ocean, *J. Geophys. Res.*, *105*, 26,117–26,134.

Gargett, A. E. (1984), Vertical eddy diffusivity in the ocean interior, *J. Mar. Res.*, *42*(2), 359–393.

Giering, R., and T. Kaminski (2003), Applying TAF to generate efficient derivative code of Fortran 77-95 programs, *Proc. Appl. Math. Mech.*, *2*(1), 54–57.

Hansen, J., et al. (2005), Earth's energy imbalance: Confirmation and implications, *Science*, *308*(5727), 1431.

Hasumi, H., and N. Suginohara (1999), Effects of locally enhanced vertical diffusivity over rough bathymetry on the world ocean circulation, *J. Geophys. Res.*, *104*, 23,364–23,374.

Hogg, N. G., G. Siedler, and W. Zenk (1999), Circulation and variability at the southern boundary of the Brazil Basin, *J. Phys. Oceanogr.*, *29*, 145–157.

Ishii, M., and M. Kimoto (2009), Reevaluation of historical ocean heat content variations with time-varying XBT and MBT depth bias corrections, *J. Oceanogr.*, *65*, 287–299.

Ishii, M., M. Kimoto, K. Sakamoto, and S. I. Iwasaki (2006), Steric sea level changes estimated from historical ocean subsurface temperature and salinity analyses, *J. Oceanogr.*, *62*(2), 155–170.

Johnson, G. C. (2008), Quantifying Antarctic Bottom Water and North Atlantic deep water volumes, *J. Geophys. Res.*, *113*, C05027, doi:10.1029/2007JC004477.

Johnson, G. C., and S. C. Doney (2006), Recent western South Atlantic bottom water warming, *Geophys. Res. Lett.*, *33*, L14614, doi:10.1029/2006GL026769.

Johnson, G. C., P. E. Robbins, and G. E. Hufford (2001), Systematic adjustments of hydrographic sections for internal consistency, *J. Atmos. Oceanic Tech.*, *18*, 1234–1244.

Johnson, G. C., S. Mecking, B. M. Sloyan, and S. E. Wijffels (2007), Recent bottom water warming in the Pacific Ocean, *J. Clim.*, *20*, 5365–5375.

Johnson, G. C., S. G. Purkey, and J. L. Bullister (2008), Warming and freshening in the abyssal southeastern Indian Ocean, *J. Clim.*, *21*, 5351–5363.

Joyce, T. M., C. Deser, and M. A. Spall (2000), The relation between decadal variability of subtropical mode water and the North Atlantic Oscillation, *J. Clim.*, *13*, 2550–2569.

Katsumata, K., and M. Fukasawa (2010), Changes in meridional fluxes and water properties in the Southern Hemisphere subtropical oceans between 1992/1995 and 2003/2004, *Prog. Oceanogr.*, doi:10.1016/j.pocean.2010.12.008, in press.

Kawano, T., M. Fukasawa, S. Kouketsu, H. Uchida, T. Doi, I. Kaneko, M. Aoyama, and W. Schneider (2006), Bottom water warming along the pathway of lower circumpolar deep water in the Pacific Ocean, *Geophys. Res. Lett.*, *33*, L23613, doi:10.1029/2006GL027933.

Kawano, T., T. Doi, H. Uchida, S. Kouketsu, M. Fukasawa, Y. Kawai, and K. Katsumata (2010), Heat content change in the Pacific Ocean between the 1990s and 2000s, *Deep Sea Res. Part II*, *57*, 1141–1151.

Kouketsu, S., M. Fukasawa, I. Kaneko, T. Kawano, H. Uchida, T. Doi, M. Aoyama, and K. Murakami (2009), Changes in water properties and transports along 24°N in the North Pacific between 1985 and 2005, *J. Geophys. Res.*, *114*, C01008, doi:10.1029/2008JC004778.

Kubota, M., N. Iwasaka, S. Kizu, M. Konda, and K. Kutsuwada (2002), Japanese ocean flux data sets with use of remote sensing observations (J-OFURO), *J. Oceanogr.*, *58*(1), 213–225.

Levitus, S., J. Antonov, and T. Boyer (2005), Warming of the world ocean, 1955–2003, *Geophys. Res. Lett.*, *32*, L02604, doi:10.1029/2004GL021592.

Levitus, S., J. I. Antonov, T. P. Boyer, R. A. Locarnini, H. E. Garcia, and A. V. Mishonov (2009), Global ocean heat content 1955–2008 in light of recently revealed instrumentation problems, *Geophys. Res. Lett.*, *36*, L07608, doi:10.1029/2008GL037155.

Lumpkin, R., and K. Speer (2007), Global ocean meridional overturning, *J. Phys. Oceanogr.*, *37*, 2555–2562.

Lyman, J. M., S. A. Good, V. V. Gouretski, M. Ishii, G. C. Johnson, M. D. Palmer, D. M. Smith, and J. K. Willis (2010), Robust warming of the global upper ocean, *Nature*, *465*, 334–337, doi:10.1038/nature09043.

Masuda, S., T. Awaji, N. Sugiura, Y. Ishikawa, K. Baba, K. Horiuchi, and N. Komori (2003), Improved estimates of the dynamical state of the North Pacific Ocean from a 4 dimensional variational data assimilation, *Geophys. Res. Lett.*, *30*(16), 1868, doi:10.1029/2003GL017604.

Masuda, S., et al. (2010), Simulated rapid warming of abyssal North Pacific waters, *Science*, *329*(5989), 319–322, doi:10.1126/science.1188703.

Matsumoto, M., and T. Nishimura (1998), Mersenne twister: A 623-dimensionally equidistributed uniform pseudo-random number generator, *ACM Trans. Model. Comput. Simul.*, *8*(1), 3–30.

Menemenlis, D., I. Fukumori, and T. Lee (2005), Using Green's functions to calibrate an ocean general circulation model, *Mon. Weather Rev.*, *133*(5), 1224–1240.

Nakano, H., and N. Suginohara (2002a), Importance of the eastern Indian Ocean for the abyssal Pacific, *J. Geophys. Res.*, *107*(C12), 3219, doi:10.1029/2001JC001065.

Nakano, H., and N. Suginohara (2002b), Effects of bottom boundary layer parameterization on reproducing deep and bottom waters in a world ocean model, *J. Phys. Oceanogr.*, *32*, 1209–1227.

NOAA (1988), Digital relief of the surface of the Earth, *Data Announce. 88-MGG-02*, Natl. Geophys. Data Cent., Boulder, Colo.

Noh, Y. (2004), Sensitivity to wave breaking and the Prandtl number in the ocean mixed layer model and its dependence on latitude, *Geophys. Res. Lett.*, *31*, L23305, doi:10.1029/2004GL021289.

Pacanowski, R. C., and S. M. Griffies (2000), The MOM 3 Manual, technical document, Geophys. Fluid Dyn. Lab., Princeton, N. J.

Purkey, S. G., and G. C. Johnson (2010), Warming of global abyssal and deep Southern Ocean between the 1990s and the 2000s: Contributions to global heat and sea level rise budgets, *J. Clim.*, *23*, 6336–6351, doi:10.1175/2010JCLI3682.1.

Rintoul, S. R. (2007), Rapid freshening of Antarctic Bottom Water formed in the Indian and Pacific oceans, *Geophys. Res. Lett.*, *34*, L06606, doi:10.1029/2006GL028550.

Roemmich, D., and J. Gilson (2009), The 2004–2008 mean and annual cycle of temperature, salinity, and steric height in the global ocean from the Argo Program, *Prog. Oceanogr.*, *82*(2), 81–100, doi:10.1016/j.pocean.2009.03.004.

Roemmich, D., J. Gilson, R. Davis, P. Sutton, S. Wijffels, and S. Riser (2007), Decadal spinup of the South Pacific subtropical gyre, *J. Phys. Oceanogr.*, *37*, 162–173.

Sloyan, B. M. (2006), Antarctic bottom and lower circumpolar deep water circulation in the eastern Indian Ocean, *J. Geophys. Res.*, *111*, C02006, doi:10.1029/2005JC003011.

Sloyan, B. M., and S. R. Rintoul (2001), The Southern Ocean limb of the global deep overturning circulation, *J. Phys. Oceanogr.*, *31*, 143–173.

Stammer, D., C. Wunsch, R. Giering, C. Eckert, P. Heimbach, J. Marotzke, A. Adcroft, C. N. Hill, and J. Marshall (2002), Global ocean circulation during 1992–1997, estimated from ocean observations and a general circulation model, *J. Geophys. Res.*, *107*(C9), 3118, doi:10.1029/2001JC000888.

Toole, J. M., and B. A. Warren (1993), A hydrographic section across the subtropical south Indian Ocean, *Deep Sea Res. Part I*, *40*, 1973–2019.

Tsujino, H., H. Hasumi, and N. Suginohara (2000), Deep Pacific circulation controlled by vertical diffusivity at the lower thermocline depths, *J. Phys. Oceanogr.*, *30*, 2853–2865.

Uchida, H., H. Yamamoto, K. Ichikawa, I. Kaneko, M. Fukasawa, T. Kawano, and Y. Kumamoto (2007), Flow of abyssal water into Wake Island Passage: Properties and transports from hydrographic surveys, *J. Geophys. Res.*, *112*, C04008, doi:10.1029/2006JC004000.

Uchida, H., H. Yamamoto, K. Ichikawa, M. Kawabe, and M. Fukasawa (2009), *Wake Island Passage Flux Experiment Data Book*, Japan Agency for Mar.-Earth Sci. and Technol., Yokosuka, Japan.

Wang, W., A. Köhl, and D. Stammer (2010), Estimates of global ocean volume transports during 1960 through 2001, *Geophys. Res. Lett.*, *37*, L15601, doi:10.1029/2010GL043949.

Warren, B. A. (1978), Bottom water transport through the Southwest Indian Ridge, *Deep Sea Res.*, *25*, 315–321.

Willis, J. K., D. Roemmich, and B. Cornuelle (2004), Interannual variability in the upper ocean heat content, temperature, and thermosteric expansion on global scales, *J. Geophys. Res.*, *109*, C12036, doi:10.1029/2003JC002260.

Yashayaev, I. (2007), Hydrographic changes in the Labrador Sea, 1960–2005, *Prog. Oceanogr.*, *73*(3–4), 242–276.

Zenk, W., and E. Morozov (2007), Decadal warming of the coldest Antarctic Bottom Water flow through the Vema Channel, *Geophys. Res. Lett.*, *34*, L14607, doi:10.1029/2007GL030340.

T. Awaji, H. Igarashi, Y. Sasaki, and N. Sugiura, Data Management and Engineering Department, Data Research Center for Marine-Earth Sciences, JAMSTEC, Yokohama 236-0001, Japan.

T. Doi, M. Fukasawa, K. Katsumata, Y. Kawai, T. Kawano, S. Kouketsu (corresponding author), S. Masuda, and H. Uchida, Research Institute for Global Change, JAMSTEC, 2-15 Natsushima-chou, Kanagawa, Yokosuka 237-0061, Japan. (skouketsu@jamstec.go.jp)

T. Toyoda, Meteorological Research Institute, 1-1 Nagamine, Tsukuba-city, Ibaraki 305-0052, Japan.